Proceedings of the  $6^{th}$  International Conference on Fluid Flow and Thermal Science (ICFFTS 2025)

Barcelona, Spain - October 29 - 31, 2025

Paper No. 119

DOI: 10.11159/icffts25.119

# Numerical Characterization of an Adsorption Heat Pump Module with Integrated Capillary Condenser-Evaporator

## Toni Maier<sup>1</sup>, Matthias Stripf<sup>1</sup>

<sup>1</sup> University of Applied Sciences Karlsruhe, Institute of Thermo-Fluid Dynamics Karlsruhe, Deutschland
Toni.Maier@h-ka.de; Matthias.Stripf@h-ka.de

**Abstract** - Hybrid heating systems, extending beyond conventional compression heat pumps, offer promising potential for reducing primary energy demand in the building sector. One effective approach involves integrating adsorption heat pumps with heat sources such as industrial waste heat or biomass boilers. These systems use high-temperature thermal energy to upgrade low-temperature ambient heat to supply medium-temperature heating networks. However, their broader adoption is often hindered by high investment costs and relatively low performance metrics. This paper presents a novel modular adsorption heat pump module (AHPM) that hermetically encapsulates all refrigeration components within a double-walled cylindrical housing. A distinctive feature of the module is a capillary-structured component integrated into the adsorber housing, which functions alternately as a condenser or an evaporator depending on the cycle phase. The operating principle of the AHPM is explained in detail. A simulation model based on mass and energy conservation equations is developed using a customized thermal network in the object-oriented Simscape language, part of the MATLAB-Simscape environment. The simulation results show a strong correlation with experimental data, with a maximum deviation of less than 8.2 % across all evaluated parameters. A comprehensive parameter analysis identifies key factors influencing system performance, particularly the average thermal output and coefficient of performance (COP). A notable finding is that the adsorption temperature has a greater impact on efficiency than the evaporation temperature. This study contributes to the advancement of compact and efficient adsorption heat pump systems for future residential energy infrastructure.

Keywords: Adsorption Heat Pump, Lumped Parameter Model, Matlab-Simscape, Parameter Analysis

#### 1. Introduction

Reducing primary energy demand is essential for achieving a sustainable energy system, particularly in the building sector, which continues to rely heavily on fossil fuels for low-temperature heat. Hybrid heating systems that combine diverse heat sources, such as biomass or industrial waste heat, with adsorption heat pumps offer considerable potential for energy savings. Adsorption heat pumps employ natural refrigerants such as water or methanol and require only a few moving parts, typically pumps and valves. As a result, they are considered quiet, reliable, and low-maintenance. The operating principle relies on the cyclic adsorption and desorption of the refrigerant on a porous solid (adsorbent), driven by the supply of high-temperature thermal energy. This process enables the transformation of low-temperature ambient heat into usable heat. Energy savings of up to 30 % have been reported [1].

Despite their potential, adsorption heat pumps have not yet achieved widespread market adoption, primarily due to their relatively low coefficient of performance (COP) and associated system costs. To overcome these limitations, research has focused on enhancing the equilibrium and kinetic properties of adsorbent-refrigerant pairs [2], [3], developing new adsorber geometries [4], [5], and exploring advanced cycle configurations using multiple adsorbers [6].

Another promising approach is to optimize the overall system design. Conventional configurations with separate evaporator and condenser units tend to require significant installation space and materials and often involve cost-intensive components such as vacuum valves or flaps. This added complexity increases manufacturing costs and reduces economic viability.

An alternative solution is to integrate the evaporator and condenser directly into the adsorber housing, forming a single, compact unit. Wittstadt et al. [7] investigated such a concept, using two identical heat exchangers, one of which was coated with a silico-aluminophosphate adsorbent. Water served as the working fluid. While the results demonstrated the viability of

the concept for heat pump applications, issues such as undesired condensation on the housing surface highlighted the need for further optimization.

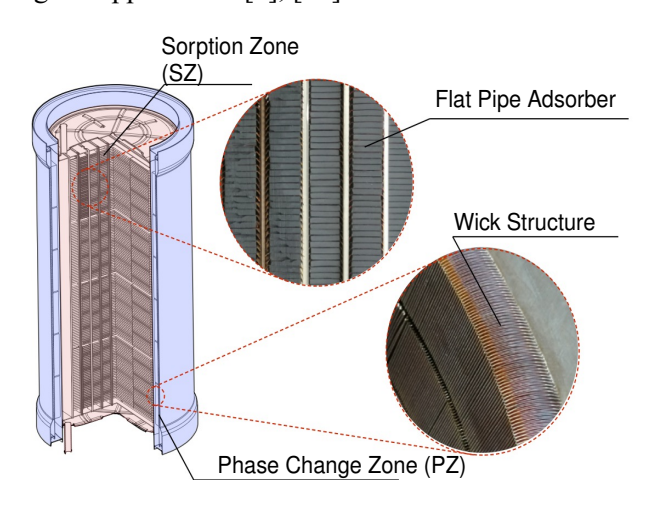
This paper presents an alternative system design proposed by [8] that addresses these challenges by integrating a capillary-structured heat exchanger into the adsorber housing, which alternately functions as a condenser or evaporator depending on the cycle phase. A validated simulation model is developed using this configuration to analyze system dynamics. The study focuses on the influence of key parameters, such as temperature levels, cycle times and volume flows, on the COP and average thermal output. The results aim to assess the potential of the proposed design to reduce system complexity while maintaining high functional performance.

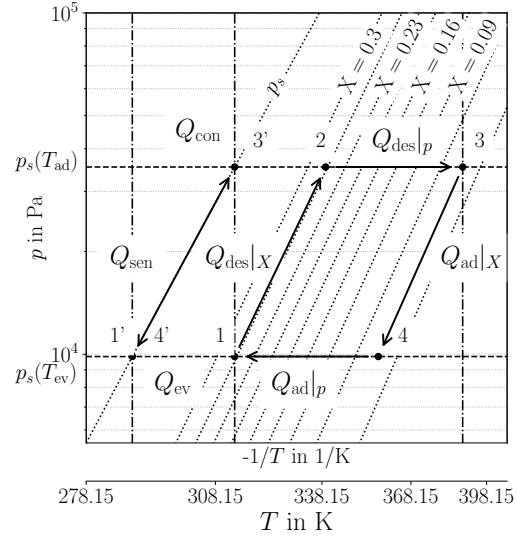
# 2. The Adsorption Heat Pump Module

#### 2.1. Design and Function

The adsorption heat pump module (AHPM), illustrated in Fig. 1a, consists of a sorption zone (SZ, red) and a phase-change zone (PZ, blue), connected via a shared refrigerant gas space (GS).

The PZ comprises a double-walled cylindrical housing with water flowing through the annular gap to either remove or supply heat during condensation and evaporation, respectively. Phase change occurs on an internal capillary (wick) structure that both increases the heat transfer surface and stores methanol, the working refrigerant. Capillary forces ensure uniform refrigerant distribution, enabling gravity-independent operation and contributing to compact system integration. The SZ contains molded activated carbon adsorbent bodies, which have been developed and characterized in previous studies [3]. For thermal coupling to the HTF, various heat exchanger configurations are possible. Maier and Stripf [9] analyzed a flat-tube geometry with stacked adsorbent bodies. In this work, an alternative design is studied in which the molded bodies are directly glued on flat heat exchanger tubes, following the approach in [3], [10].





(a) Design of the Adsorption heat pump module

**(b)** Clapeyron diagram of an adsorption heat

Fig. 1: Design and the thermodynamic function in a Clapeyron-diagram of the adsorption heat pump module

The SZ is supplied with heat transfer fluid (HTF) at a temperature of  $T_{\rm des} \approx 388$  K during desorption and a temperature of  $T_{\rm ad} \approx 303-323$  K during adsorption. Simultaneously, the PZ is maintained at  $T_{\rm con} = T_{\rm ad} \approx 303-323$  K during condensation, and  $T_{\rm ev} \approx 288$  K during evaporation. Unlike conventional systems, no vacuum valves are required, as all switching is achieved via fluid control valves that adjust HTF flow and temperature. The internal pressure follows the saturated vapor pressure corresponding to the temperature of the PZ.

The thermodynamic cycle is illustrated in the Clapeyron diagram (Fig. 1b) for the representative values  $T_{\text{des}} = 388 \text{ K}$ ,  $T_{\text{ad}} = T_{\text{con}} = 313 \text{ K}$ , and  $T_{\text{ev}} = 288 \text{ K}$ . In this  $\log(p)$  vs.-1/T representation, the equilibrium loading lines appear as straight

lines. The temperature in Kelvin is given on the secondary axis. The equilibrium is modeled using the Dubinin-Astakhov equation [11]:

 $X_{\text{eq}} = \rho W_0 \exp \left[ -\left( \frac{R_{\text{uni}} T}{E M} \ln \left( \frac{p_s(T_{\text{ads}})}{n} \right) \right)^n \right]$ (1)

where  $W_0$  is the maximum specific pore volume, E the characteristic energy,  $R_{\rm uni}$  the universal gas constant, M the molar mass,  $p_s$  the saturation pressure at  $T_{ads}$ ,  $\rho$  the density of adsorbed methanol (approximated using saturated liquid data), and  $X_{\text{eq}}$  the equilibrium loading [kg refrigerant/kg adsorbent]. Parameters  $W_0$ , E and n are based on experimental data from [3].

The dashed and dash-dotted lines in Fig. 1b indicate relevant pressure and temperature levels. The cycle starts at states 1/1', where both SZ and PZ are isosterically heated by the HTF, supplying sensible heat  $Q_{\text{sen}}$  and initiating desorption heat  $Q_{\text{des}|X}$  reaching states 2/2'. Desorption then continues isobarically with  $Q_{\text{des}|p}$  supplied to the adsorber while methanol desorbs and condenses in the PZ, releasing  $Q_{con}$ . Once equilibrium is reached (state 3), both zones are cooled simultaneously and the internal pressure drops. The system releases heat ( $Q_{\text{sen}}$  and  $Q_{\text{ad}|X}$ ) to the corresponding HTF until reaching states 4/4'. During the subsequent isobaric adsorption,  $Q_{\text{ad}|p}$  is removed from the adsorber, and methanol evaporates in the PZ using environmental heat  $Q_{\text{ev}}$ . The heat released during adsorption and condensation can be used for space heating system, improving the overall system efficiency.

#### 2.2. Figures of Merit

To evaluate the efficiency of the module, the coefficient of performance (COP) is calculated based on the integrated heat flows over a full operating cycle, rather than instantaneous power values. This approach is necessary because the heat pump operates in alternating transient modes [12]. The heating COP<sub>h</sub> is defined by:

$$COP_{h} = \frac{Q_{ads/X} + Q_{ads/p} + Q_{con} - Q_{sens}}{Q_{des/X} + Q_{des/p}}$$
(2)

where the terms represent the integrated heat quantities associated with adsorption  $(Q_{\text{ad}|X}, Q_{\text{ad}|p})$ , condensation  $(Q_{\text{con}})$ , sensible heat losses ( $Q_{\text{sens}}$ ), and desorption ( $Q_{\text{des}|X}$ ,  $Q_{\text{des}|p}$ ).

These energy quantities are derived from energy balances over the SZ and the PZ, using the HTF mass flow rates  $\dot{m}_{\rm SZ}$ and  $\dot{m}_{\rm PZ}$ , the specific heat capacity  $c_p$ , and the inlet and outlet temperatures, respectively. For the SZ during the adsorption part of the cycle, the heat is calculated as:

part of the cycle, the heat is calculated as:
$$Q_{\text{ads/X}} + Q_{\text{ads/p}} = \int_{\tau + \chi t_{\text{cyc}}}^{\tau + t_{\text{cyc}}} \dot{m}_{\text{SZ,in}} c_{p, \text{SZ, in}} T_{\text{SZ,out}} c_{p, \text{SZ, out}} T_{\text{SZ,out}} dt$$
and for the PZ during the desorption/condensation cycle part:
$$\sigma^{\tau + \chi t_{\text{cyc}}}$$
(3)

$$Q_{\rm con} - Q_{\rm sens} = \int_{-\tau}^{\tau + \chi t_{\rm cyc}} \dot{m}_{\rm PZ,in} \, c_{p,\,\rm PZ,\,in} \, T_{\rm PZ,in} - \dot{m}_{\rm PZ,out} \, c_{p,\,\rm PZ,\,out} \, T_{\rm PZ,out} \, {\rm d}t \tag{4}$$
 The desorption heat is computed using Eq. 3, but with integration limits corresponding to those in Eq. 4 (i.e. the first

half-cycle). Here,  $t_{\rm cyc}$  denotes the total duration of one full operating cycle and  $\chi = t_{\rm des}/t_{\rm cycle}$  the desorption ratio. These equations account for changes in HTF properties - especially specific heat capacity - due to significant temperature variations between inlet and outlet, which are particularly pronounced during the transitions between adsorption/evaporation and desorption/condensation phases.

The average thermal output  $Q_h$  per cycle is calculated by summing the adsorption and condensation heat contributions and dividing by the cycle time:

$$Q_{\rm h} = \frac{Q_{\rm ads/X} + Q_{\rm ads/p} + Q_{\rm con} - Q_{\rm sens}}{t_{\rm cvc}}$$
 (5)

### 3. Modeling

#### 3.1. Assumptions and System Description

The modeling of the adsorption heat pump module (AHPM) is based on the conservation equations for mass and energy. To reduce complexity and computational effort, a number of simplifying assumptions are made, as listed in Table 1.

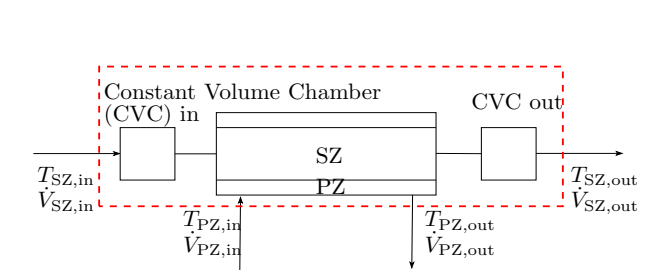
Tab. 1 Model assumptions used for the simulation

#### **Thermal Assumptions**

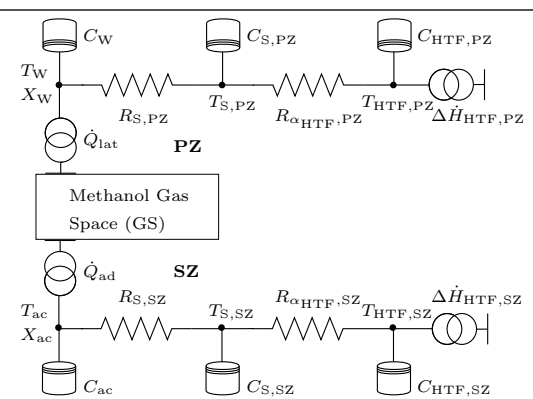
- 1. The module is adiabatic to the environment.
- 2. Uniform temperature in the PZ (capillary, inner cylinder, fluid).
- 3. Uniform temperature in the SZ (carbon, solid, fluid).
- 4. Heat transfer between SZ and PZ occurs solely via methanol vapor transport.

#### Geometric and Fluid Assumptions

- 5. The unadsorbed vapor behaves as an ideal gas.
- 6. Axial temperature gradients along the module are neglected.
- 7. Inlet/outlet volumes of the PZ are considered negligible.
- 8. Mass transfer resistance within the activated carbon is neglected.



(a) System of the simulation model with boundary conditions for the AHPM



**(b)** Thermal network of the AHPM for the sorption zone, phase change zone, and the connecting gas space

Fig. 2: Schematic overview of the AHPM system and its thermal network.

A schematic representation of the simulated system and its thermal network is shown in Fig. 2. The red dashed rectangle in Fig. 2a defines the system boundary for the simulation. The inlet and outlet volumes of the SZ are modelled using the Constant Volume Chamber (CVC) block from the Simscape Thermal Liquid library. The core of the simulation model, which includes the SZ and PZ, is implemented in the object-oriented Simscape language and is described in more detail in Section 3.2.

The boundary conditions for the simulation are the volume flow rates  $V_{\rm SZ,in}$  and  $V_{\rm PZ,in}$ , and the corresponding inlet temperatures  $T_{\rm SZ,in}$  and  $T_{\rm PZ,in}$ . These are implemented as ideal sources from the Thermal Liquid library. Outlet values are computed by the model.

#### 3.2. Mathematical Modelling

The model divides the system into thermal networks representing the SZ and PZ, coupled through a shared methanol gas space (GS). The corresponding thermal network structure is depicted in Fig. 2b. Temperatures are calculated at each node (solid node: index S; heat transfer fluid: index HTF; activated carbon: index ac; wick structure: index W). Each node's temperature evolution is governed by heat capacities C, conduction resistances  $R_{\rm S}$ , convection resistances  $R_{\rm a}$ , and heat sources including adsorption heat  $Q_{\rm ad}$ , latent heat  $Q_{\rm lat}$ , and enthalpy flow difference  $\Delta H_{\rm HTF}$  due to HTF transport within the PZ and SZ. The heat sources due to adsorption and the latent heat are modeled using specific enthalpies for adsorption  $\Delta h_{\rm ad}$  and

phase change  $\Delta h_{\rm v}$  as follow

$$Q_{\text{lat}} = \begin{cases} \dot{m}_{\text{CH}_3\text{OH, PZ}} \Delta h_{\text{v}} & \text{if } T_{\text{GS}} > T_{\text{sat, W}} \\ \dot{m}_{\text{CH}_3\text{OH, PZ}} \Delta h_{\text{v}} + \dot{m}_{\text{CH}_3\text{OH, PZ}} c_{p, \text{CH}_3\text{OH}}^{\text{g}} \left( T_{\text{GS}} - T_{\text{sat, W}} \right) & \text{if } T_{\text{GS}} > T_{\text{sat, W}} \\ Q_{\text{ad}} = \dot{m}_{\text{CH}_3\text{OH, SZ}} \Delta h_{\text{ad}} & (7) \end{cases}$$

$$Q_{\rm ad} = \dot{m}_{\rm CH_2OH, SZ} \Delta h_{\rm ad} \tag{7}$$

Eq. 6 distinguishes between evaporation (first case) and condensation (second case). In the condensation case, the second term accounts for the sensible heat associated with the superheated methanol vapor, where  $c_{p, \text{ CH}_2\text{OH}}^g$  is the specific heat capacity of methanol vapor.

The mass flows of methanol to and from the PZ and SZ, denoted as  $\dot{m}_{\rm CH_3OH,\ PZ}$  and  $\dot{m}_{\rm CH_3OH,\ SZ}$ , respectively, are determined by the mass of the wick structure  $m_W$ , the mass of the activated carbon  $m_{ac}$ , and their respective loading change rates  $\frac{dX}{dt}$ :

$$\dot{m}_{\text{CH}_3\text{OH, PZ}} = m_{\text{W}} \frac{\text{d}X_{\text{W}}}{\text{d}t'},\tag{8}$$

$$\dot{m}_{\text{CH}_3\text{OH, SZ}} = m_{\text{ac}} \frac{dX_{\text{ac}}}{dt}.$$
(9)

For activated carbon, the rate of adsorption or desorption is modeled using the linear driving force (LDF) model [13]:

$$\frac{\mathrm{d}X_{\mathrm{ac}}}{\mathrm{d}t} = K_{\mathrm{LDF}} \left( X_{\mathrm{eq, ac}} - X_{\mathrm{ac}} \right),\tag{10}$$

where  $K_{\rm LDF}$  is a kinetic time constant,  $X_{\rm eq,ac}$  is the equilibrium loading from Eq. 1, and  $X_{\rm ac}$  is the instantaneous loading. The rate of loading change in the wick structure is determined by equating Eq. 6 with Newton's law of cooling, yielding:

$$\frac{dX_{W}}{dt} = \begin{cases}
\frac{\alpha_{\text{CH}_{3}\text{OH,PZ}_{ev}} A_{\text{ref}} (T_{GS} - T_{W})}{m_{W} \Delta h_{v}} \\
\alpha_{\text{CH}_{3}\text{OH,PZ}_{con}} A_{\text{ref}} (T_{GS} - T_{W}) \\
\hline m_{W} (\Delta h_{v} + c_{p,\text{CH}_{3}\text{OH}}^{g} (T_{GS} - T_{W}))
\end{cases} (11)$$

Here, the lateral surface of the inner cylinder defines the reference surface  $A_{ref}$ . Previous studies on finned tubes suggest that the evaporation heat transfer coefficient  $\alpha_{\text{CH3OH,PZev}}$  remains nearly constant until the wick structure approaches dryness, assuming natural convection as the primary mechanism [14]. In this study, it is therefore set constant at  $\alpha_{\text{CH3OH,PZev}} = 950$ W/(m<sup>2</sup>K). This value is lower than reported by [14] due to the differences in geometry and the lower latent heat of methanol compared to water.

A phenomenological approach is adopted for the condensation heat transfer coefficient  $\alpha_{\text{CH3OH,PZcon}}$ , accounting for the influence of wick loading:

$$\alpha_{\text{CH}_3\text{OH},PZ_{\text{con}}} = 1450 \exp[-35.5 X_{\text{W}}]$$
 (12)

These models for the heat transfer coefficients during evaporation and condensation are approximated; detailed fundamental studies are required to precisely describe heat transfer mechanisms within the wick structure.

Temperature evolution at each node and in the gas space is governed by the transient energy balance

$$C\frac{\mathrm{d}T}{\mathrm{d}t} = \sum Q \sum H \tag{13}$$

where C represents the thermal capacity at the node. While Eq. 13 assumes time-invariant material data for simplicity, loading-dependent heat capacities of the wick and activated carbon are updated after each time step. Additionally, mass conservation in the gas space and the ideal gas law are simultaneously solved.

For numerical initialization, adsorption/evaporation equilibrium is assumed, with an initial 1 % deviation of the activated carbon loading below equilibrium. This minor deviation stabilizes calculation across different boundary conditions. The total methanol mass in the AHPM is set to 2.4 kg.

#### 3.3. Experimental Validation of the Modell

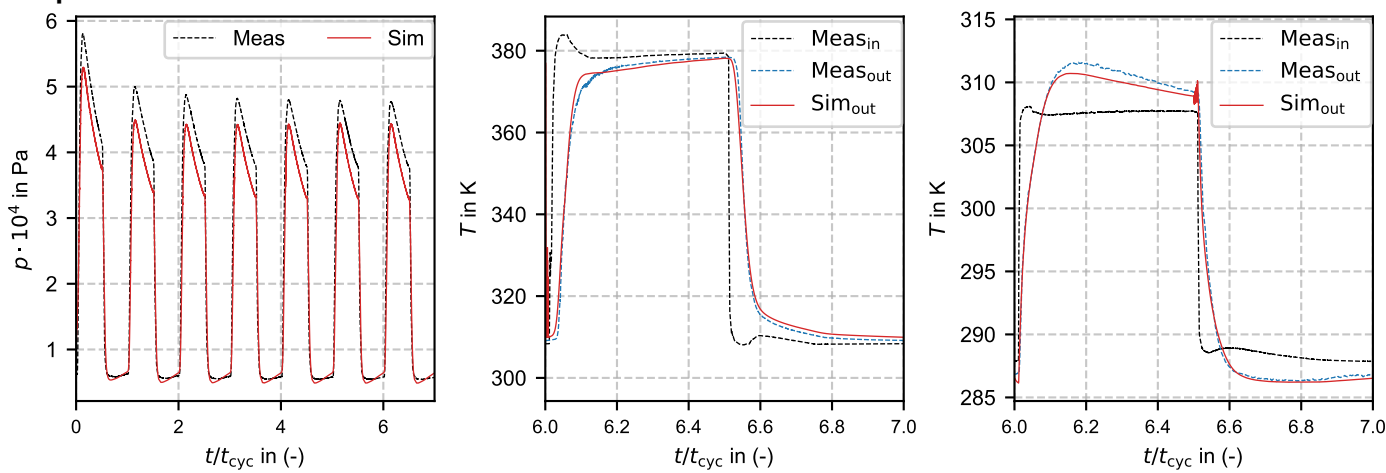
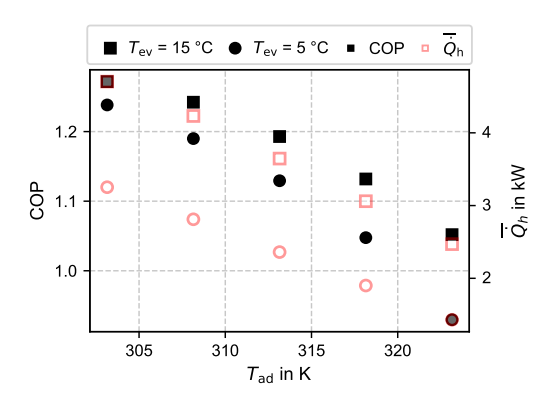


Fig. 3: Comparison of measurement and model simulation left pressure of gas space, middle SZ and right PZ inlet/outlet temperatures

To validate the simulation model, an experimental setup was developed to measure inlet and outlet conditions as well as the gas-phase pressure within the module. Volume flow rates in the test bench are measured using two Siemens Sitrans F M MAG sensors for the desorption and evaporation fluid circuits and a Kobold MIK sensor for the adsorption circuit. The sensors are positioned to match the flow conditions of the respective zones (SZ and PZ). Temperatures are recorded with 3-wire PT100 sensors. All experimental data are digitized using a National Instruments cDAQ-9178 acquisition system at a sampling interval of 0.05 s, enabling accurate capture of steep transient temperature gradients. Target temperatures for the validation tests are set to  $T_{\rm des} = 378.15$  K,  $T_{\rm ad} = 308.15$  K, and  $T_{\rm ev} = 288.15$  K. Figure 3 compares simulation results with measurements of the gas-space pressure and inlet/outlet temperatures. All data sets initially exhibit decaying transient behavior that stabilizes after approximately five cycles. This behavior is clearly visualized in the pressure plot. Starting from cycle six, a stable periodic behavior is observed, which is analyzed in detail in the temperature plots. The simulated PZ outlet temperature is slightly underestimated during condensation and in the later stages of evaporation. Similarly, the simulated SZ outlet temperature is slightly underestimated, except at the beginning of desorption, and marginally overestimated during adsorption. These discrepancies could be attributed to factors such as fluid inhomogeneities and sensor lag. The evaporation process is nearly isobaric, whereas the non isobaric condensation process suggests a heat transfer bottleneck in the PZ.

The accuracy of the simulation model is quantitatively assessed by calculating the standard deviation  $\sigma$  between simulation and measurement, following the approach of [15]. The resulting values are  $\sigma(T_{SZ,out}) = 2.34\%$ ,  $\sigma(T_{PZ,out}) = 2.23\%$ , and  $\sigma(p_{GS}) = 8.17\%$ , indicating sufficient agreement and highlighting opportunities for further parameter refinement.

### 4. Results of the Parameter Analysis



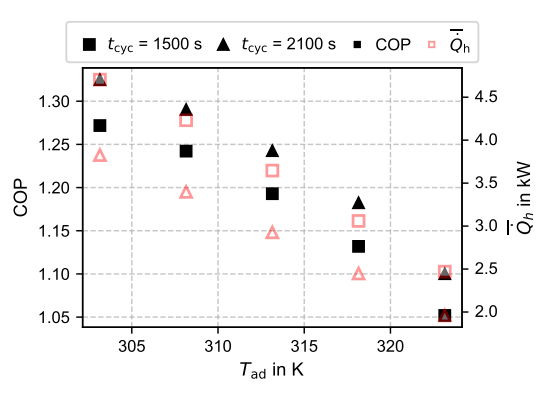
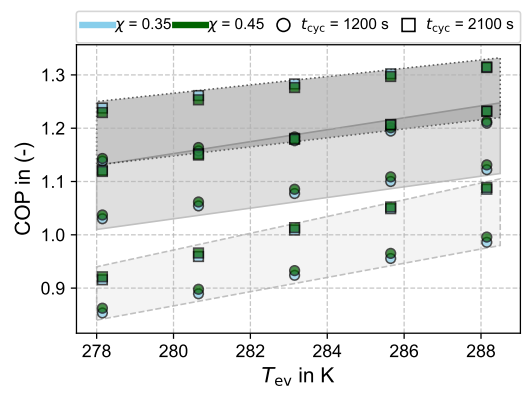


Fig 4: Influence of  $T_{ad}$  on COP  $Q_h$  and at a fixed volumetric flow rate of 30 l/min. Left: variation with evaporation temperatures. Right: variation with cycle time.

A parameter study is conducted with operating conditions chosen to reflect typical scenarios for building heating applications. The desorption temperature is fixed at  $T_{\rm des}$  = 388.15 K, while the adsorption temperature ranges from 303.15 to 323.15 K and the evaporation temperature from 278.15 to 288.15 K. HTF volume flow rates vary between 15 and 30 l/min, the desorption ratio  $\chi$  between 0.35–0.5, and cycle times  $t_{\rm cyc}$  from 1200 to 2100 s.

Fig. 4 illustrates the variation of COP and average heat output  $Q_h$  with adsorption temperature for different evaporation temperatures and cycle times. Both COP and  $Q_h$  improve as adsorption temperature decreases and evaporation temperature increases. However, increasing the cycle time results in a reduced average heat output  $Q_h$  but an improved COP (Fig. 4, right). Therefore, the optimal cycle time is a trade-off between maximizing COP and satisfying the required average heat output of the target application. Figure 5 further explores COP dependency on evaporation temperature at different volume flow rates.



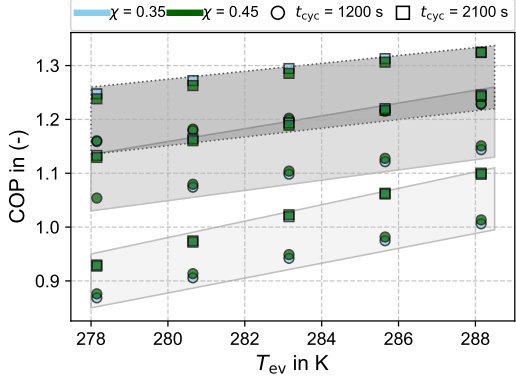


Fig 5: Parameter analysis of COP variation with evaporation temperature and cycle time at different volumetric flow rates (left: V = 20 l/min; right: V = 30 l/min). The shaded parallelograms represent constant adsorption temperatures: light gray for 303.15 K, medium gray for 313.15 K, and dark gray for 323.15 K.

Constant adsorption temperature is illustrated with parallelograms in light gray for 303.15 K and in gray and dark gray for 313.15 K and 323.15 K, respectively. Increasing volumetric flow leads to a slight rise in COP, though the rate of increase diminishes at longer cycle times. This trend suggests that both longer cycle durations and higher volume flows allow the

system to more closely approach theoretical equilibrium conditions, thereby limiting further gains. The desorption ratio  $\chi$  influences COP, although to a lesser extent than other parameters. However, systems with pronounced mass-transfer limitations might exhibit stronger sensitivity to  $\chi$ . Due to the clear interactions observed between the desorption ratio and other parameters, further detailed investigations are recommended, particularly regarding its use in system control strategies.

Additionally, Fig. 5 illustrates that COP can drop below unity at higher adsorption and lower evaporation temperatures, primarily due to substantial heat losses during cyclic temperature transitions. Such losses can be mitigated in multi-module systems employing heat recovery cycles. Moreover, the achievable temperature lift ( $\Delta T_{\rm lft} = T_{\rm ad} - T_{\rm ev}$ ) for a COP > 1 is more sensitive to variations in adsorption temperature than evaporation temperature. Therefore, reducing the adsorption temperature should be prioritized for improved efficiency, as it enables a larger refrigerant loading range between adsorption and desorption.

#### 5. Conclusion

This study introduces a novel adsorption heat pump module (AHPM) featuring an integrated capillary-structured heat exchanger that serves as both evaporator and condenser. A validated theoretical model was developed, demonstrating close agreement with experimental data. The calculated COP values underline the AHPM's suitability for integration into hybrid heating systems in building applications. A comprehensive parameter analysis examined the effects of adsorption and evaporation temperatures, cycle time, heat exchanger flow rate, and desorption ratio. The key findings are:

- 1. COP and average heat output are highly sensitive to variations in adsorption and evaporation temperatures, as well as to cycle times. Thus, careful optimization of these parameters is crucial for maximizing performance.
- 2. Increasing evaporation temperatures and decreasing adsorption temperatures significantly improve both COP and heat output, emphasizing the benefit of temperature-level optimization.
- 3. Longer cycle times increase COP but reduce total heat output, indicating a trade-off between efficiency and capacity.
- 4. Higher heat exchanger volumetric flow rates slightly improve COP and heat output.
- 5. The desorption ratio exhibits a minor influence on COP but may play a valuable role in refining control strategies, particularly in systems experiencing significant mass transfer limitations.
- 6. Adsorption temperature affects COP more strongly than evaporation temperature, making it the critical factor for system performance optimization.

By introducing and thoroughly evaluating this novel module design, the study contributes to enhancing the practical feasibility and economic viability of adsorption heat pump systems. Although the initial results are promising, further research on the complete system including advanced heat recovery strategies is required to accelerate commercial adoption.

#### **Acknowledgements**

Financial support from the Ministry of Economic Affairs, Labor and Tourism of the state government of Baden-Württemberg (Germany) within the investBW program (Grant No. BW1\_2083/02) and the Deutsche Bundesstiftung Umwelt (Grant No. 38442/01) are gratefully acknowledged.

#### References

- [1] F. Meunier, "Adsorption heat powered heat pumps," *Applied Thermal Engineering*, vol. 61, no. 2, pp. 830–836, 2013.
- [2] H. Hassan, A. Mohamad, Y. Alyousef, and H. Al-Ansary, "A review on the equations of state for the working pairs used in adsorption cooling systems," *Renewable and Sustainable Energy Reviews*, vol. 45, pp. 600–609, May 2015.
- [3] O. Kraft, "Adsorber-compounds für mobile und stationäre adsorptionswärmepumpen mit hoher leistungsdichte," Ph.D. thesis, Fakultät für Maschinenwesen Technische Universität Dresden, 2021
- [4] S. Metcalf, Z. Tamainot-Telto, and R. Critoph, "Application of a compact sorption generator to solar refrigeration: Case study of dakar (senegal)," *Applied Thermal Engineering*, vol. 31, no. 14, pp. 2197–2204, Oct. 2011.
- [5] M. M. Saleh, R. Al-Dadah, S. Mahmoud, E. Elsayed, and O. El-Samni, "Wire fin heat exchanger using aluminium fumarate for adsorption heat pumps," *Applied Thermal Engineering*, vol. 164, p. 114 426, Jan. 2020.
- [6] Q. Pan, R. Wang, and L. Wang, "Comparison of different kinds of heat recoveries applied in adsorption refrigeration

- system," International Journal of Refrigeration, vol. 55, pp. 37–48, Jul. 2015.
- [7] U. Wittstadt, G. Füldner, E. Laurenz, A. Warlo, A. Große, R. Herrmann, L. Schnabel and W. Mittelbach, "A novel adsorption module with fiber heat exchangers: Performance analysis based on driving temperature differences," *Renewable Energy*, vol. 110, pp. 154–161, Sep. 2017.
- [8] R. Burk and L. Ludwig, "Sorptionswärmeübertragungsmodul," German patent app. DE 102018212820A1, Mar. 2019.
- [9] T. Maier and M. Stripf, "Distributed parameter model of a novel heat pump adsorber design using 3D-FEM," *Applied Thermal Engineering* vol. 278, Nov. 2025,
- [10] O. Kraft, M. Stripf, and U. Hesse, "Heat and mass transfer in activated carbon composites with artificial macro pores for heat pump applications," *Adsorption*, vol. 25, no. 6, pp. 1121–1133, Aug. 2019.
- [11] M. M. Dubinin and V. A. Astakhov, "Development of the concepts of volume filling of micropores in the adsorption of gases and vapors by microporous adsorbents: Communication 1. carbon adsorbents," *Bulletin of the Academy of Sciences of the USSR Division of Chemical Science*, vol. 20, no. 1, pp. 3–7, Jan. 1971.
- [12] D. B. Boman, A. W. Raymond, and S. Garimella, *Adsorption Heat Pumps: Fundamentals and Applications* (Mechanical Engineering Series). Cham: Springer International Publishing, 2021, ISBN: 978-3-030-72179-4 978-3-030-72180-0.
- [13] M. H. Chahbani, J. Labidi, and J. Paris, "Effect of mass transfer kinetics on the performance of adsorptive heat pump systems," *Applied Thermal Engineering*, 2002.
- [14] G. B. Abadi and M. Bahrami, "Combined evaporator and condenser for sorption cooling systems: A steady-state performance analysis," *Energy*, vol. 209, p. 118 504, Oct. 2020.
- [15] M. Schicktanz and T. Núñez, "Modelling of an adsorption chiller for dynamic system simulation," *International Journal of Refrigeration*, vol. 32, no. 4, pp. 588–595, Jun. 2009.